Electronic Supplementary Information

Fabrication of Amorphous Subnanometric Palladium Nanostructures on Metallic Transition Metal Dichalcogenides for Efficient Hydrogen Evolution Reaction

Liang Mei[1#], Yuefeng Zhang[1#], Zimeng Ye[1], Ting Han[1], Honglu Hu, Ruijie Yang[1], Ting Ying[1], Weikang Zheng[1], Ruixin Yan[1], Yue Zhang[1], Zhenbin Wang[1], Zhiyuan Zeng[1,2]*

[1]Department of Materials Science and Engineering and State Key Laboratory of Marine Pollution, City University of Hong Kong, Hong Kong, People's Republic of China.

[2] Shenzhen Research Institute, City University of Hong Kong, Shenzhen 518057, China

Corresponding authors:

Z.Y. Zeng (zhiyzeng@cityu.edu.hk)

These authors contributed equally: Liang Mei, Yuefeng Zhang

Contents

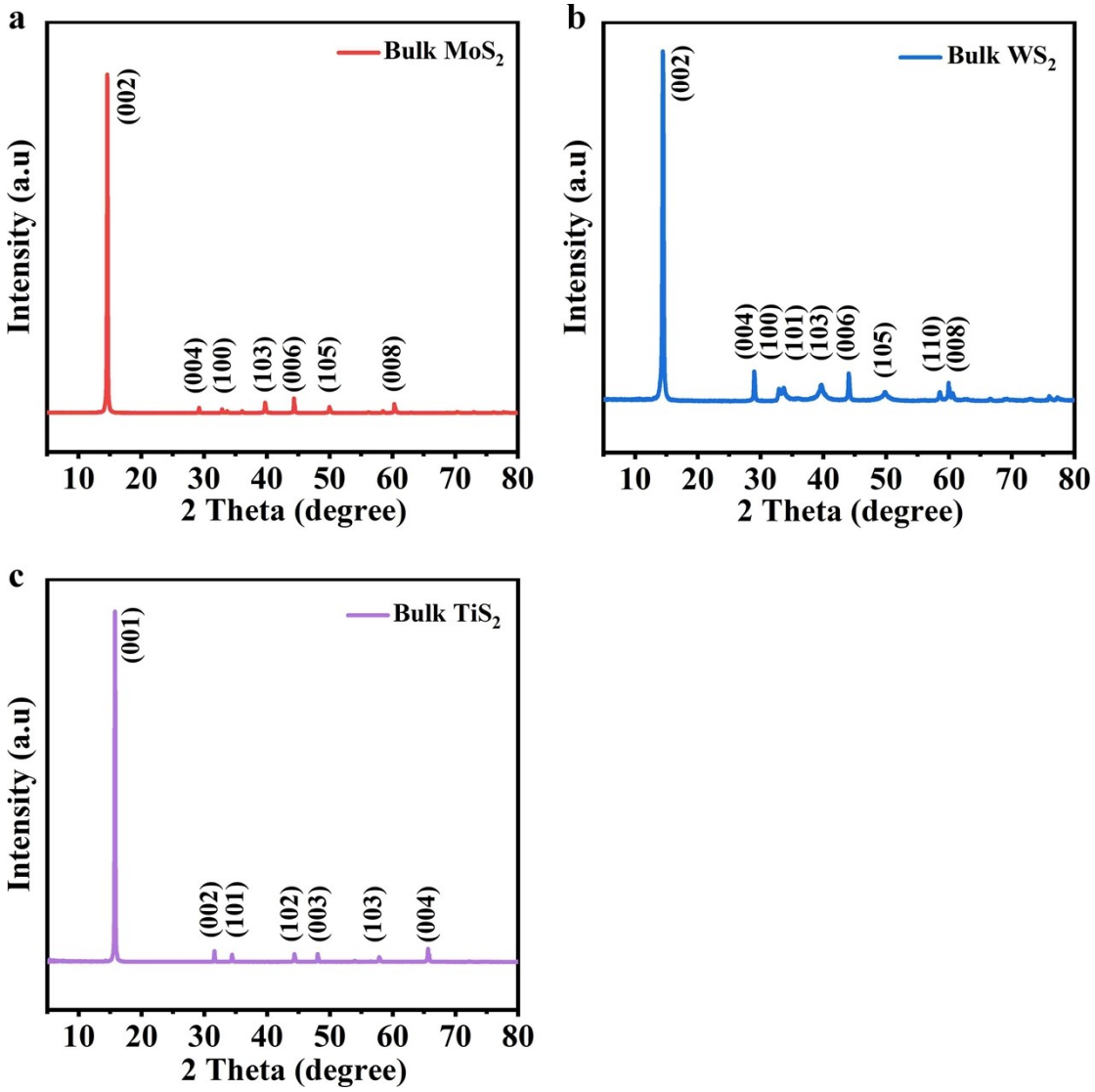

Fig. S1 | XRD spectra of bulk MoS_2 (**a**), bulk WS_2 (**b**) and bulk TiS_2 (**c**). The high purity phase of bulk MoS_2, WS_2, TiS_2 are confirmed; the peaks detected in bulk MoS_2, bulk WS_2, and bulk TiS_2 can be well indexed to MoS_2-PDF#06-0097, WS_2-PDF#08-0237, and TiS_2-PDF#15-0853. The strongest peak that corresponding to (002) plane of MoS_2 and WS_2, as well as (001) plane of TiS_2 indicate their layered structures.

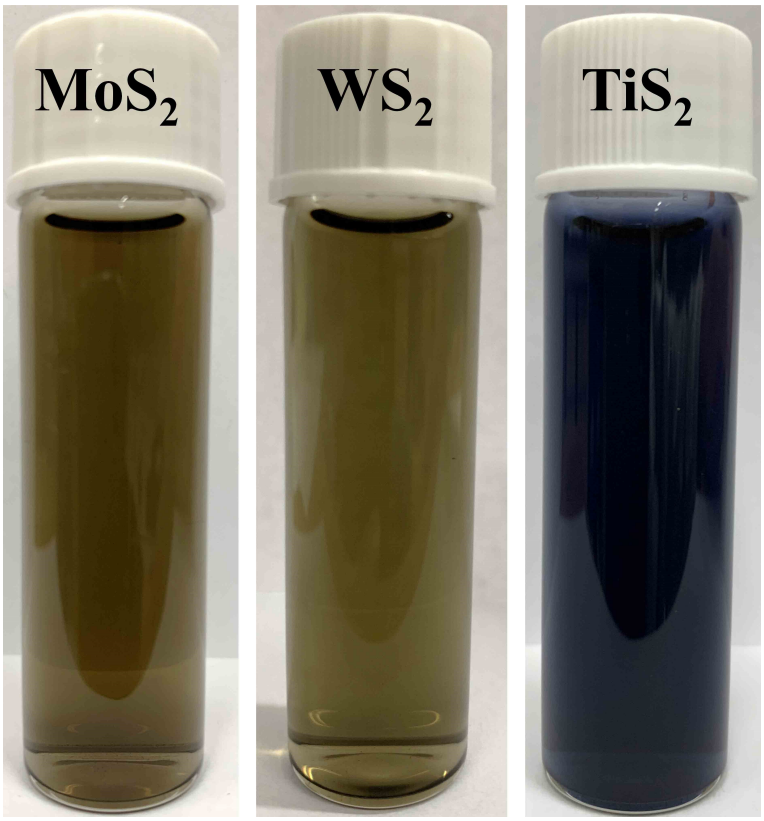

Fig. S2 | Photographs of exfoliated MoS_2 nanosheets (**a**), WS_2 nanosheets (**b**) and TiS_2 nanosheets (**c**) dispersed in DI water. All these TMD nanosheets are well dispersed in DI water.

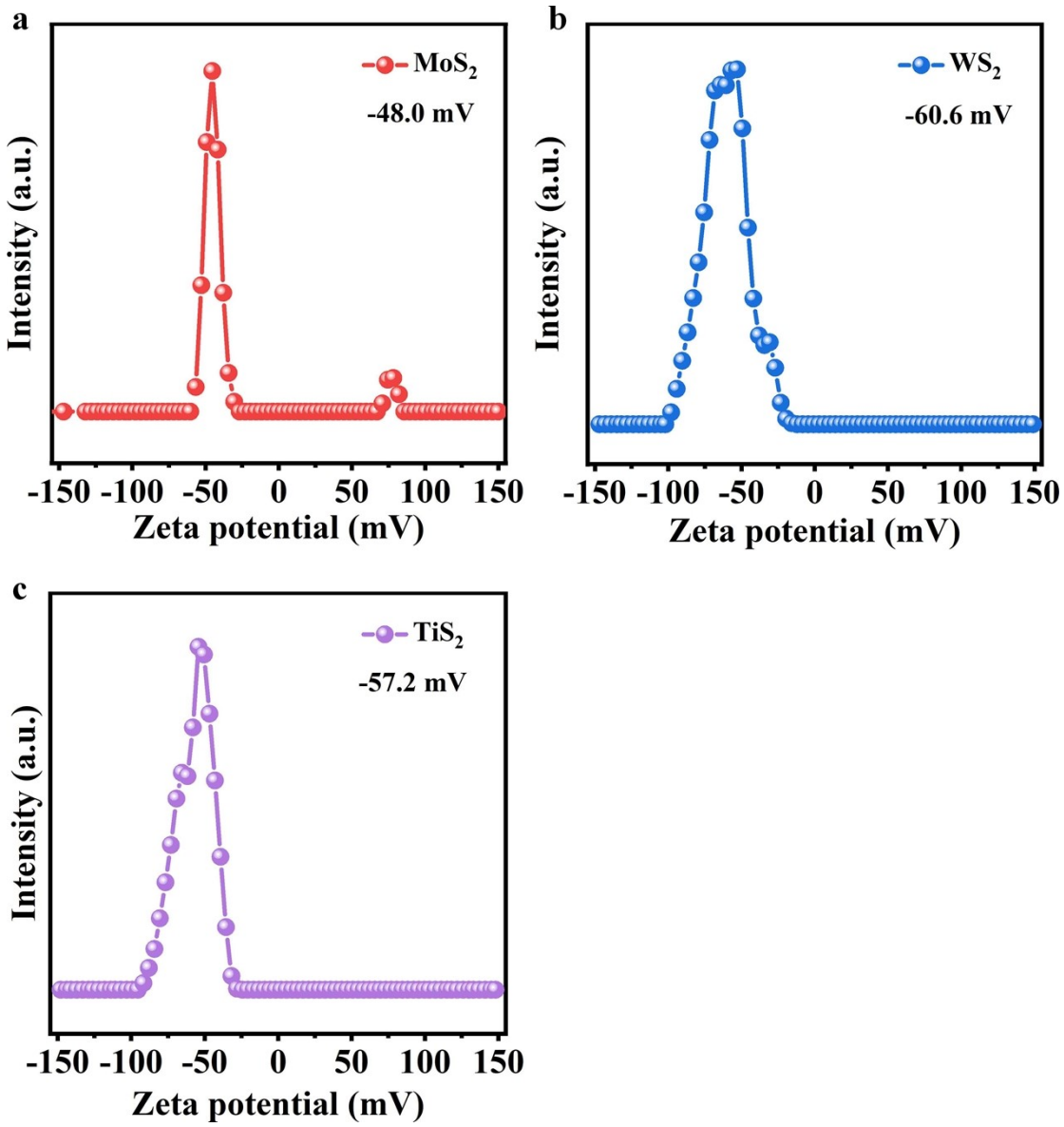

Fig. S3 | Zeta potential of exfoliated MoS_2 nanosheets solution (**a**), exfoliated WS_2 nanosheets solution (**b**) and exfoliated TiS_2 nanosheets solution (**c**). All the MoS_2, WS_2, and TiS_2 nanosheets solution exhibit a negative charge in DI water, which enables their well dispersibility in DI water via electrostatic repulsion.

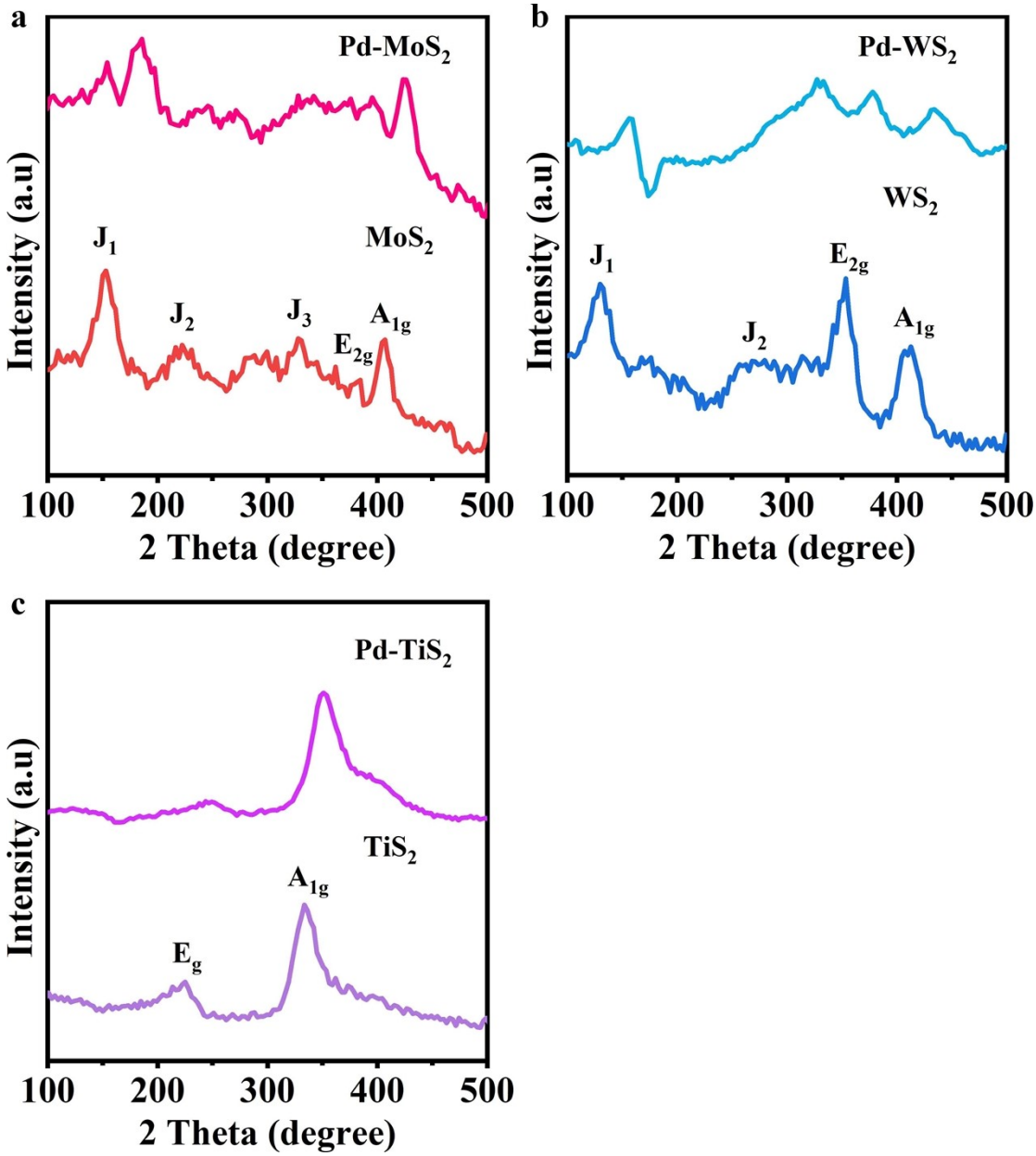

Fig. S4 | Raman spectra of MoS_2 and Pd-MoS_2 (**a**), WS_2 and Pd-WS_2 (**b**), TiS_2 and Pd-TiS_2 (**c**) nanosheets.

Peaks at 152 cm^{-1}, 223 cm^{-1}, 329 cm^{-1} are corresponding to J_1, J_2, J_3 of metallic (1T or 1T′) MoS_2, while the peaks at 381 cm^{-1} and 406 cm^{-1} are attributed to the E_{2g} and A_{1g} of semiconducting MoS_2 (**Fig. S4a**). Peaks at 131 cm^{-1}, 271 cm^{-1}, 385 cm^{-1} are corresponding to J_1, J_2, J_3 of metallic (1T or 1T′) WS_2, while the peaks at 353 cm^{-1} and 410 cm^{-1} are attributed to the E_{2g} and A_{1g} of semiconducting WS_2 (**Fig. S4b**). Peaks at 224 cm^{-1} and 334 cm^{-1} are corresponding to E_g and A_{1g} of 1T TiS_2 (**Fig. S4c**).

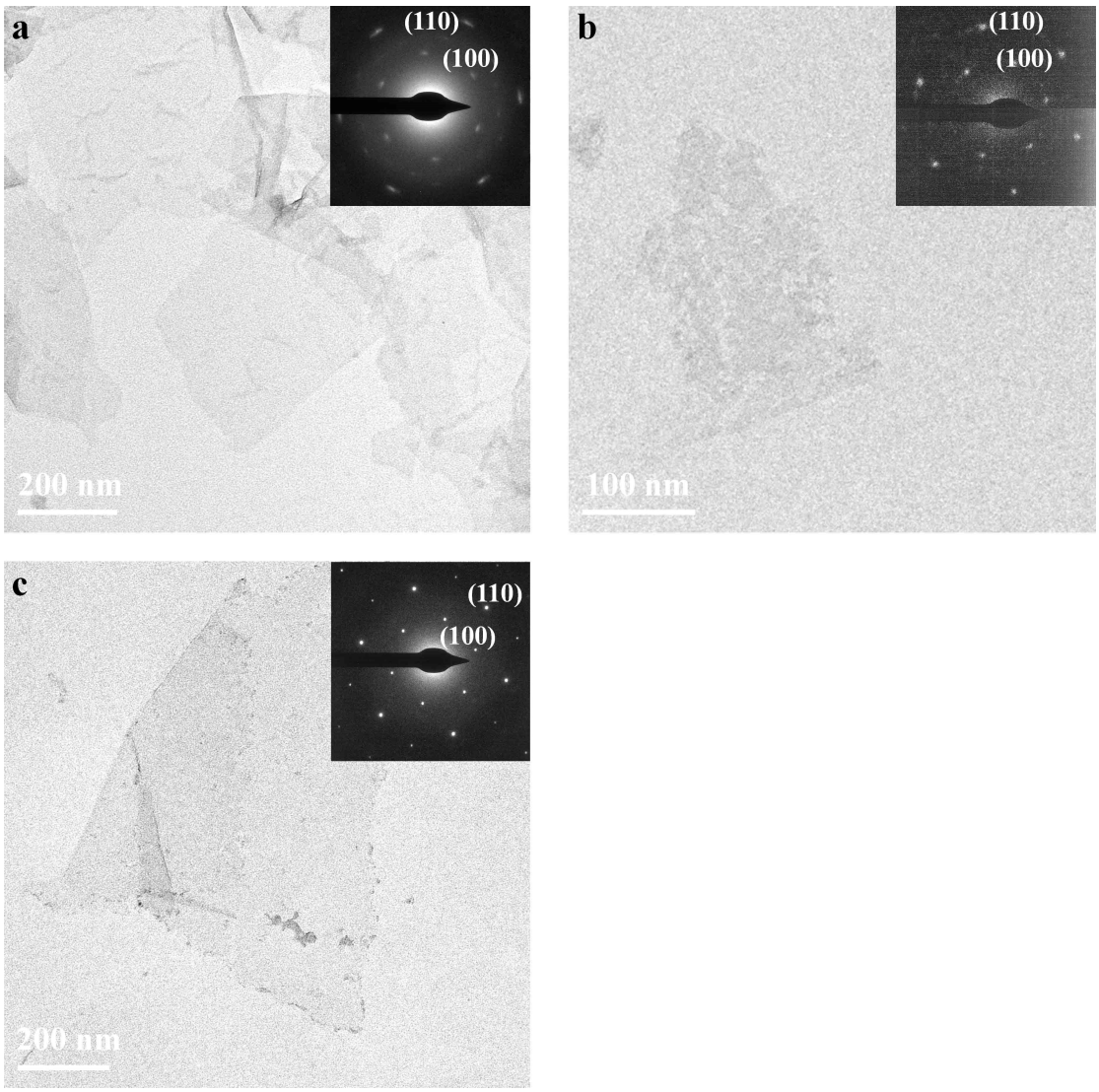

Fig. S5 | TEM images of exfoliated MoS_2 nanosheets (**a**), exfoliated WS_2 nanosheets (**b**) and exfoliated TiS_2 nanosheets (**c**). The insets show the diffraction patterns. All the MoS_2, WS_2, and TiS_2 nanosheets exhibit nanosheets morphology and good crystallinity.

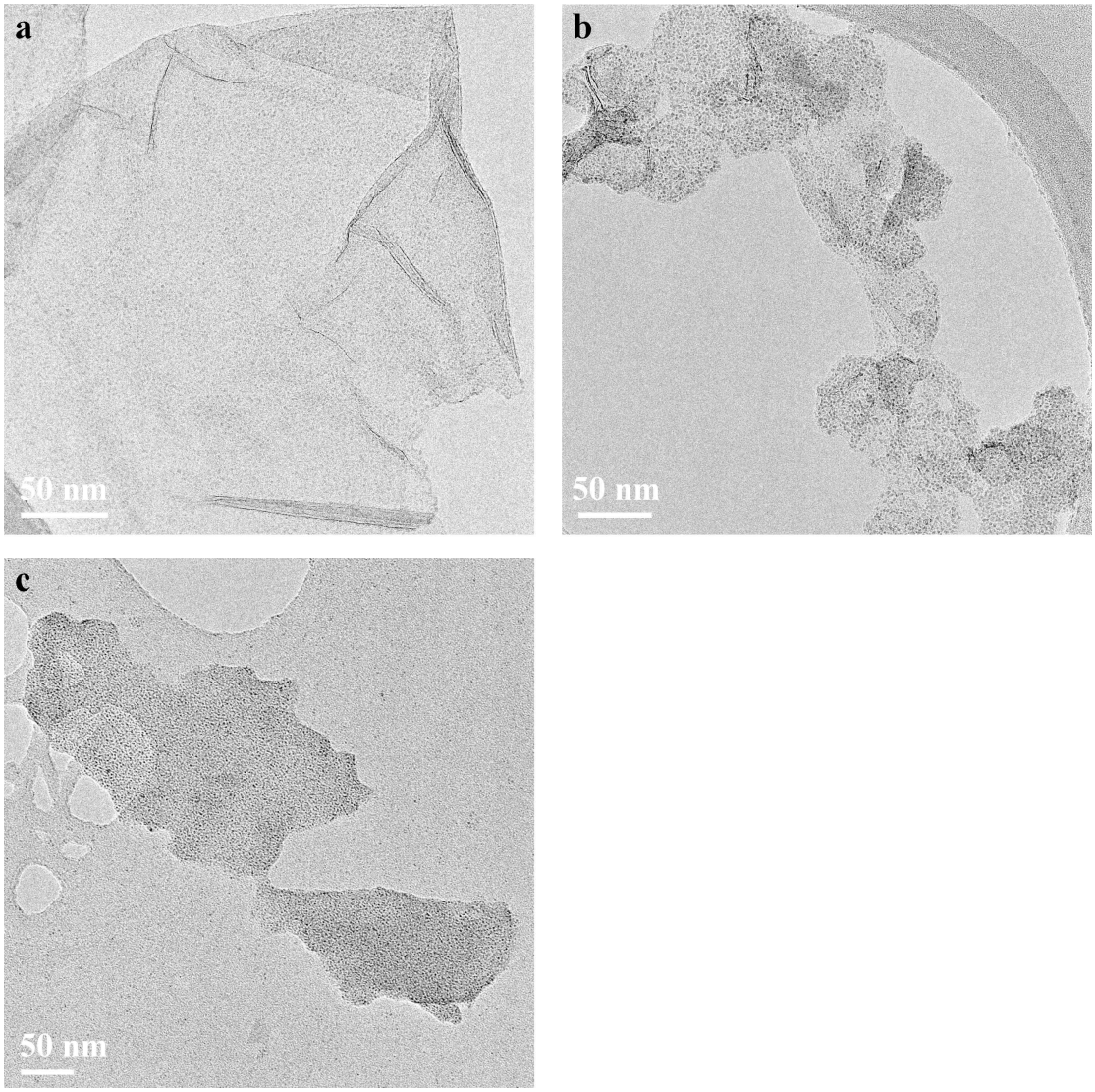

Fig. S6 | TEM images of Pd-MoS_2 (**a**), Pd-WS_2 (**b**) and Pd-TiS_2 (**c**) composites. The monodispersed Pd nanoparticles are densely decorated onto each TMD nanosheets.

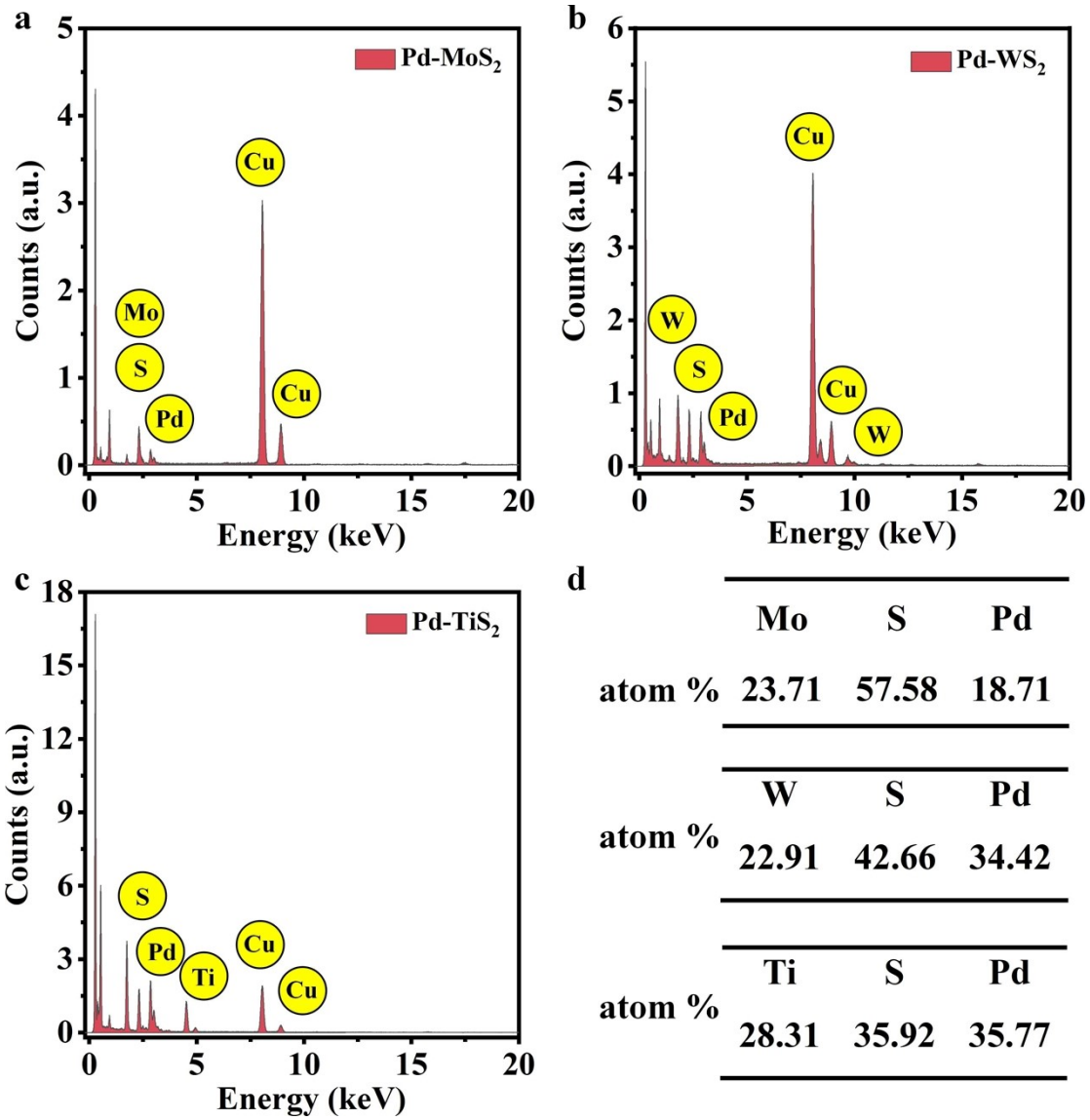

Fig. S7 | EDS spectra of Pd-MoS_2 (**a**), Pd-WS_2 (**b**) and Pd-TiS_2 (**c**) composites. The atomic ration for each element in Pd-TMD composites are shown in (**d**).

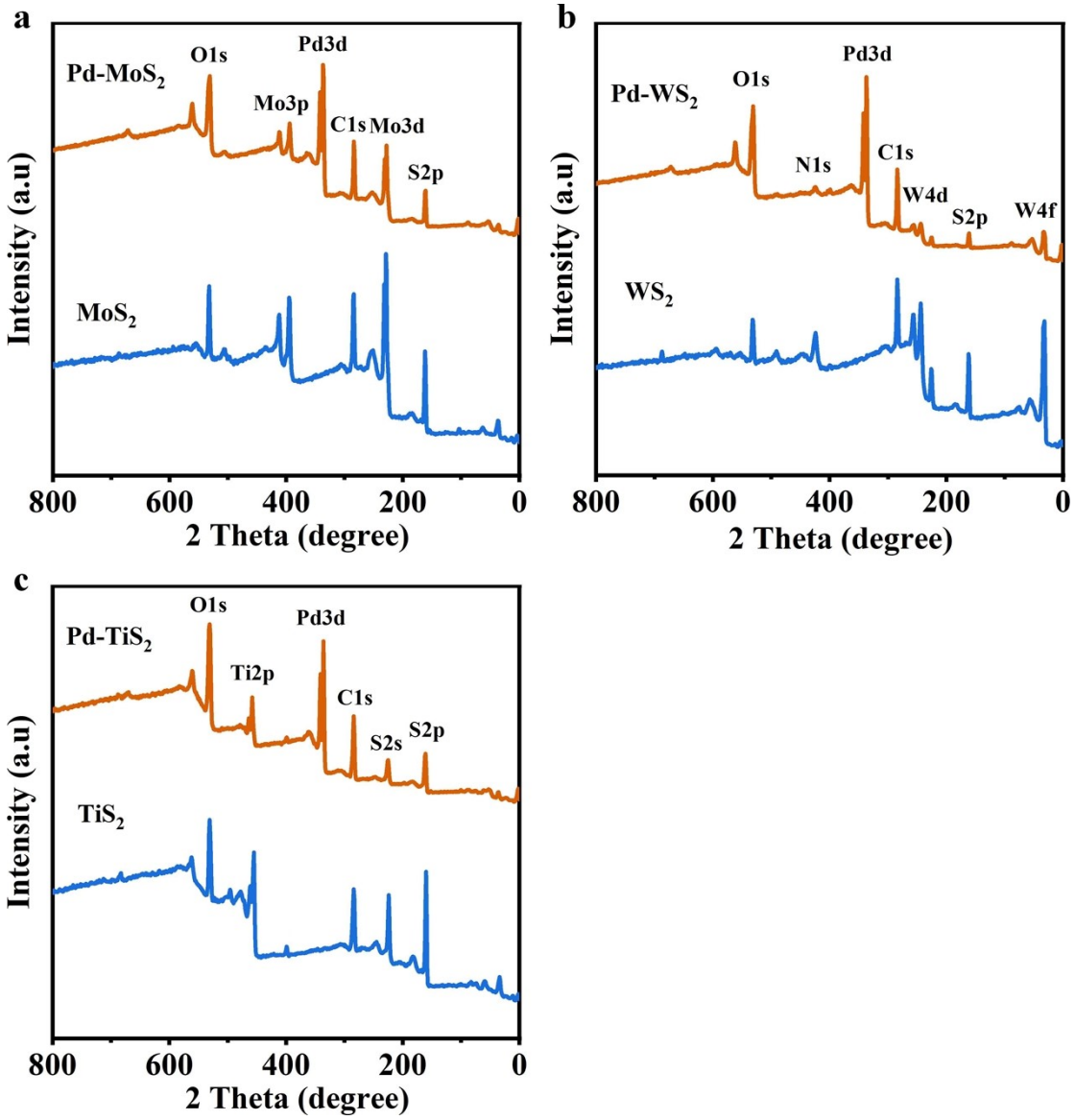

Fig. S8 | XPS full spectra of Pd-MoS_2 and pristine MoS_2 (**a**), Pd-WS_2 and pristine WS_2 (**b**), Pd-TiS_2 and pristine TiS_2 (**c**). All the Pd-TMD composites exhibit strong Pd3d signal compared with pristine TMD.

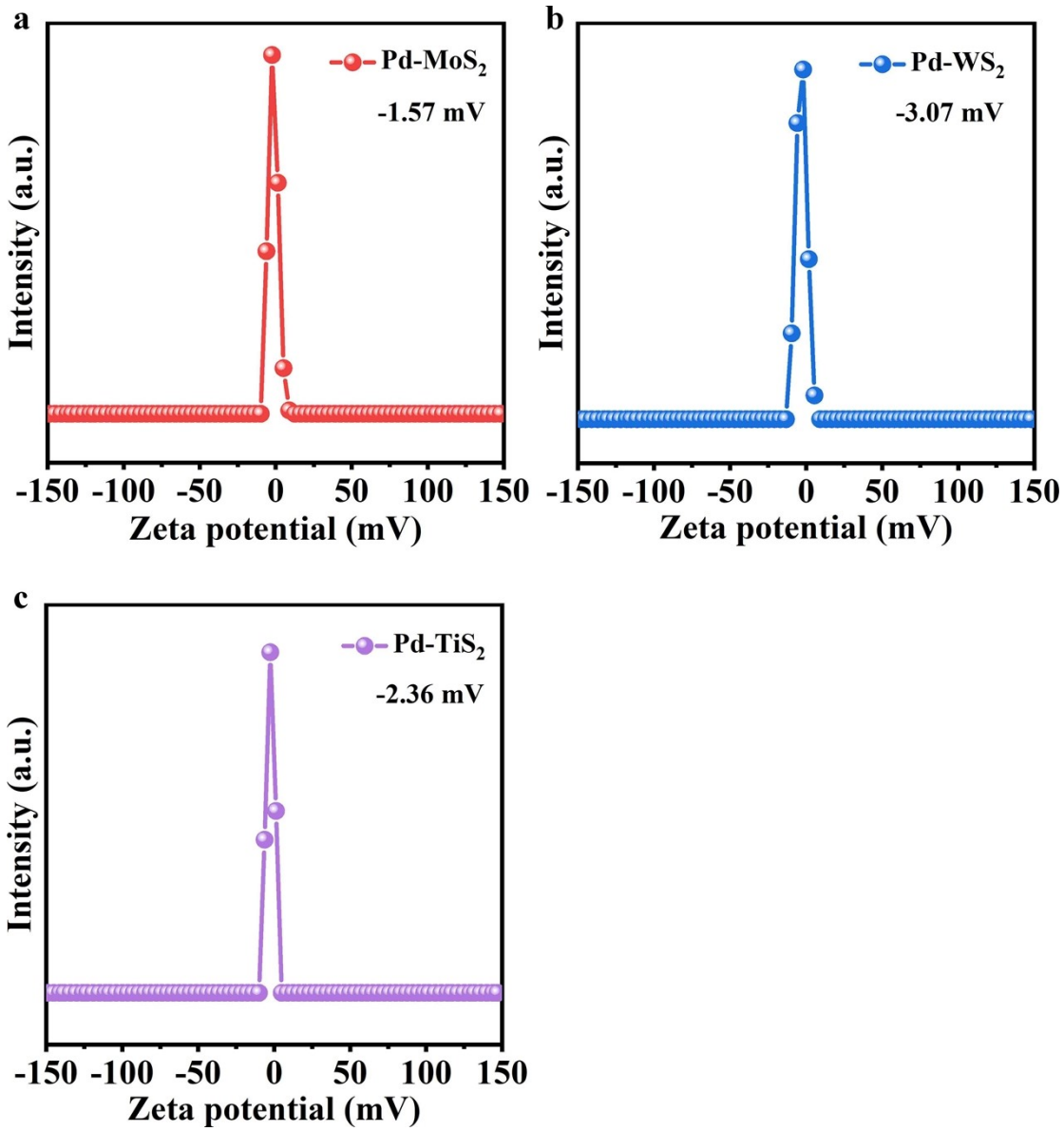

Fig. S9 | Zeta potential of Pd-MoS_2 (**a**), Pd-WS_2 (**b**) and Pd-TiS_2 solution (**c**).

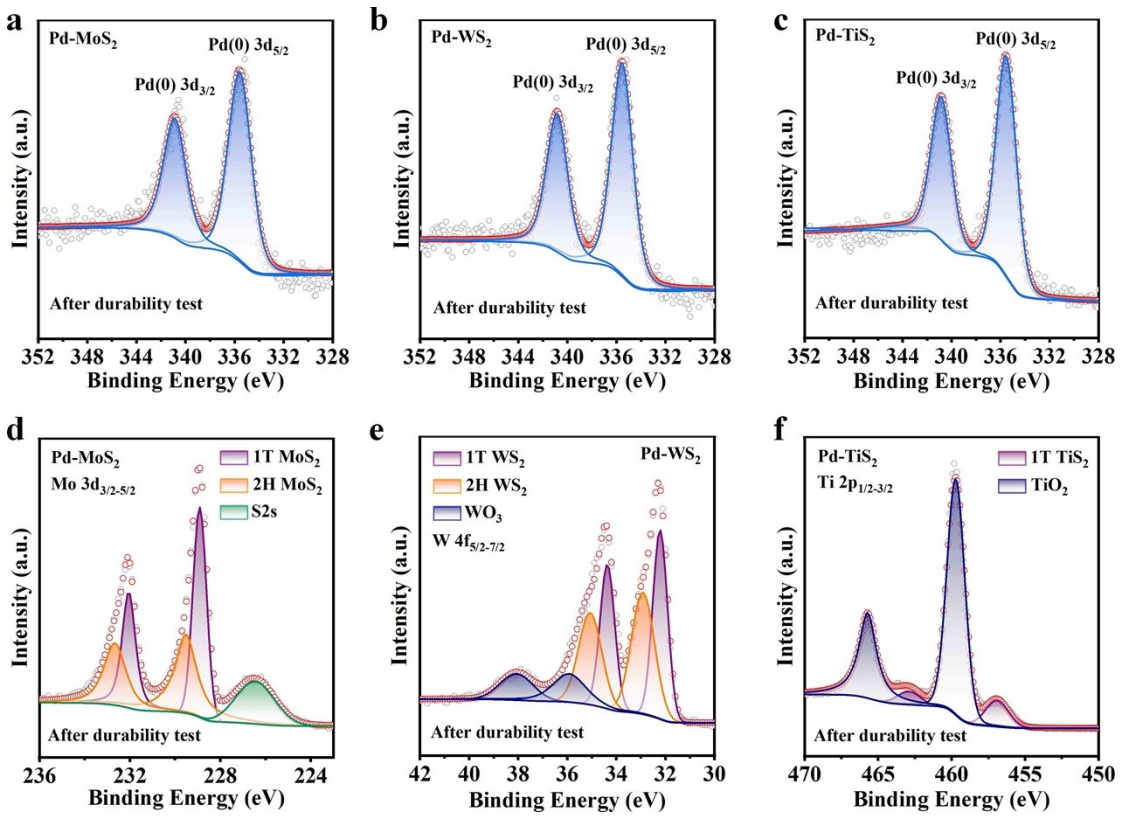

Fig. S10 | The XPS data for Pd 3d (**a-c**), Mo 3d (**d**), W 4f (**e**), and Ti 2p (**f**) of Pd-MoS_2, Pd-WS_2, and Pd-TiS_2 after durability test.

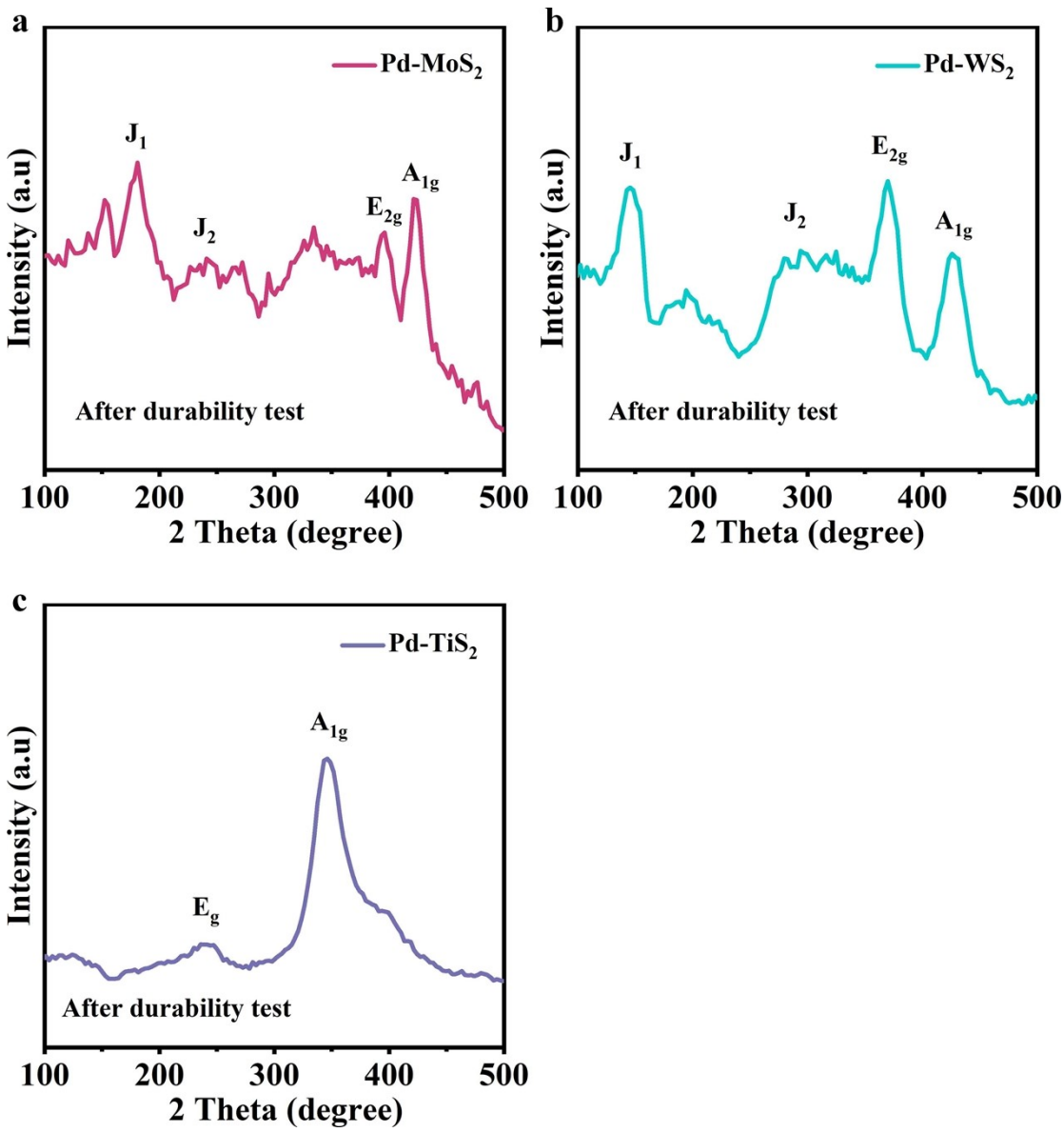

Fig. S11 | The Raman spectra of Pd-MoS_2, Pd-WS_2, and Pd-TiS_2 after durability test.

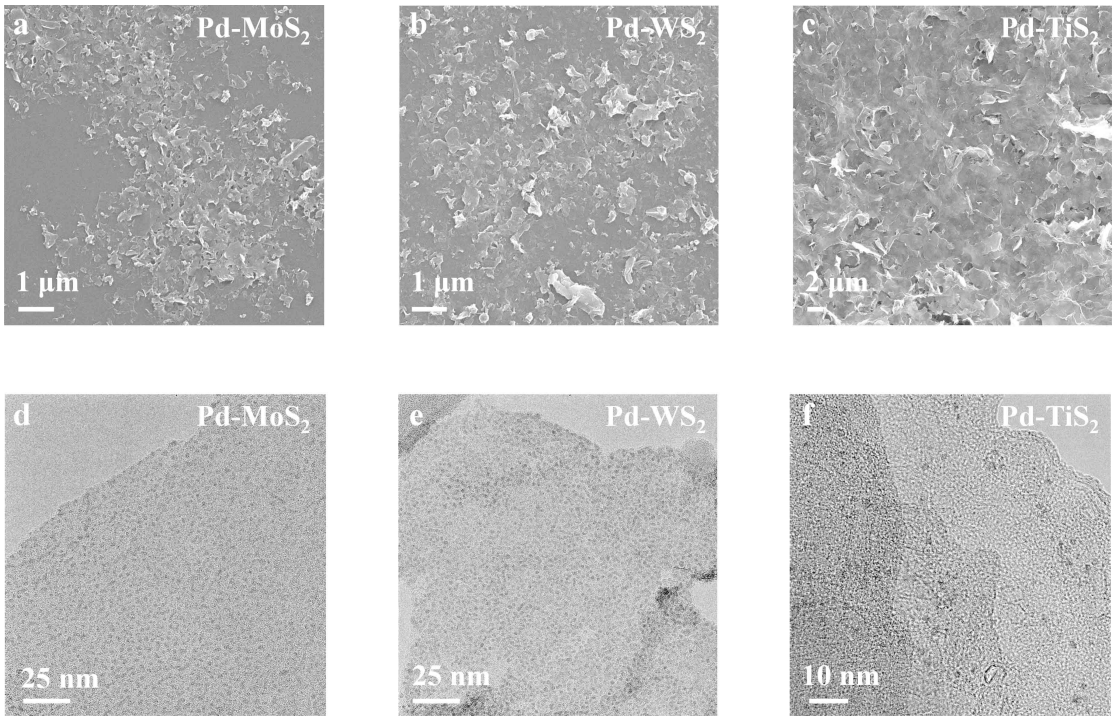

Fig. S12 | SEM images of Pd-MoS_2 (**a**), Pd-WS_2 (**b**), and Pd-TiS_2 (**c**) after durability test. The corresponding HRTEM images are shown in (**d-f**).

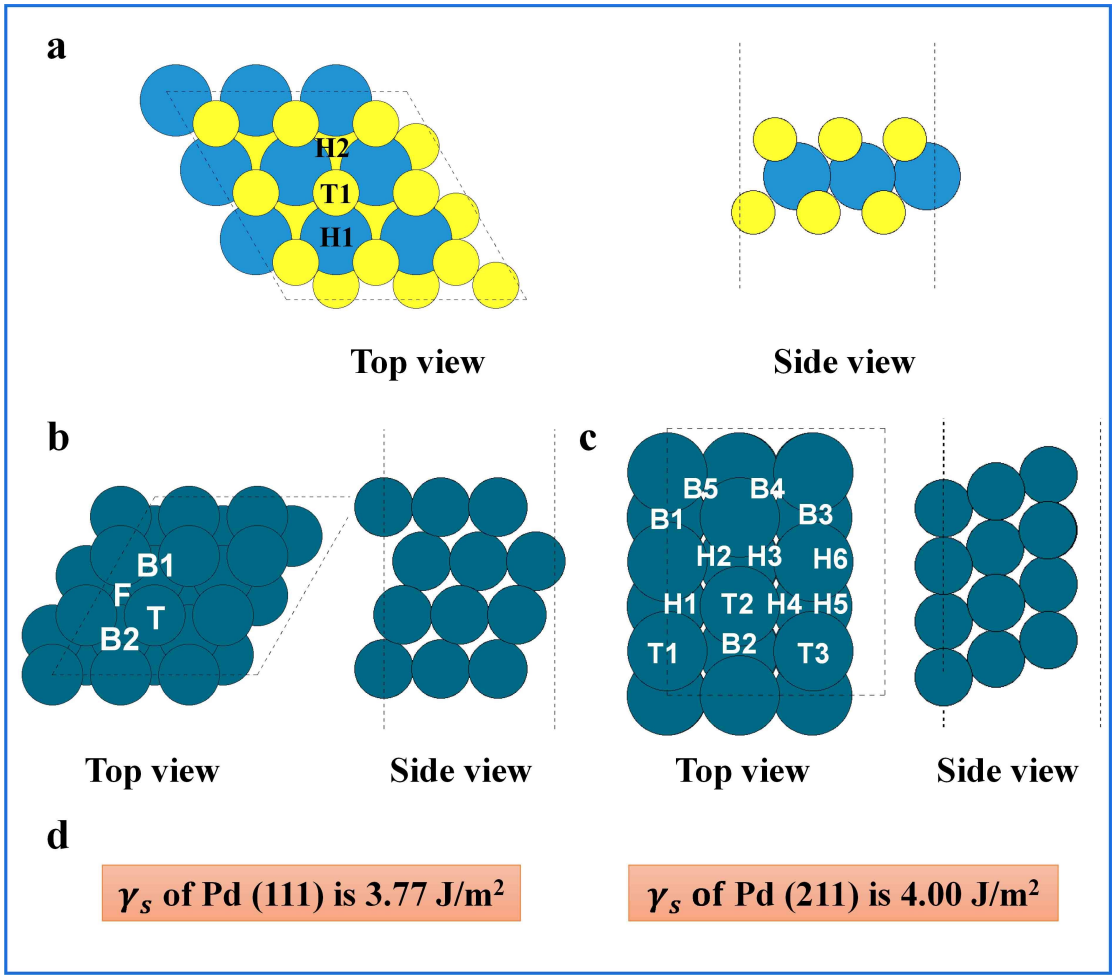

Fig. S13 | Model diagrams and possible H adsorption sites for TMD (**a**), Pd (111) (**b**), and Pd (211) (**c**). Surface energy value of Pd (111) and Pd (211) (**d**).

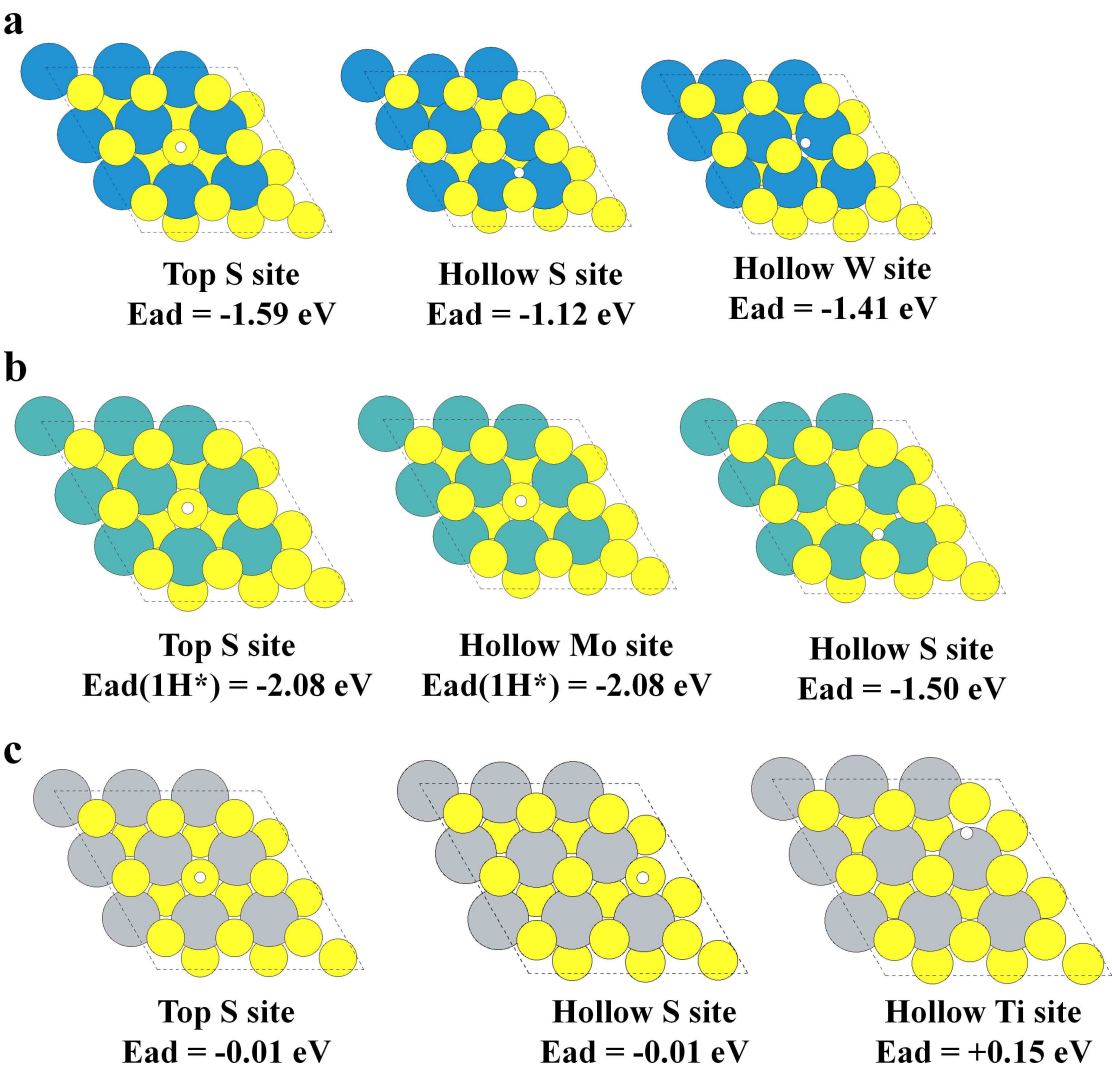

Fig. S14 | The most stable adsorption models and corresponding adsorption energy values for H adsorbed on different sites of TiS_2 (**a**), WS_2 (**b**), and MoS_2 (**c**).

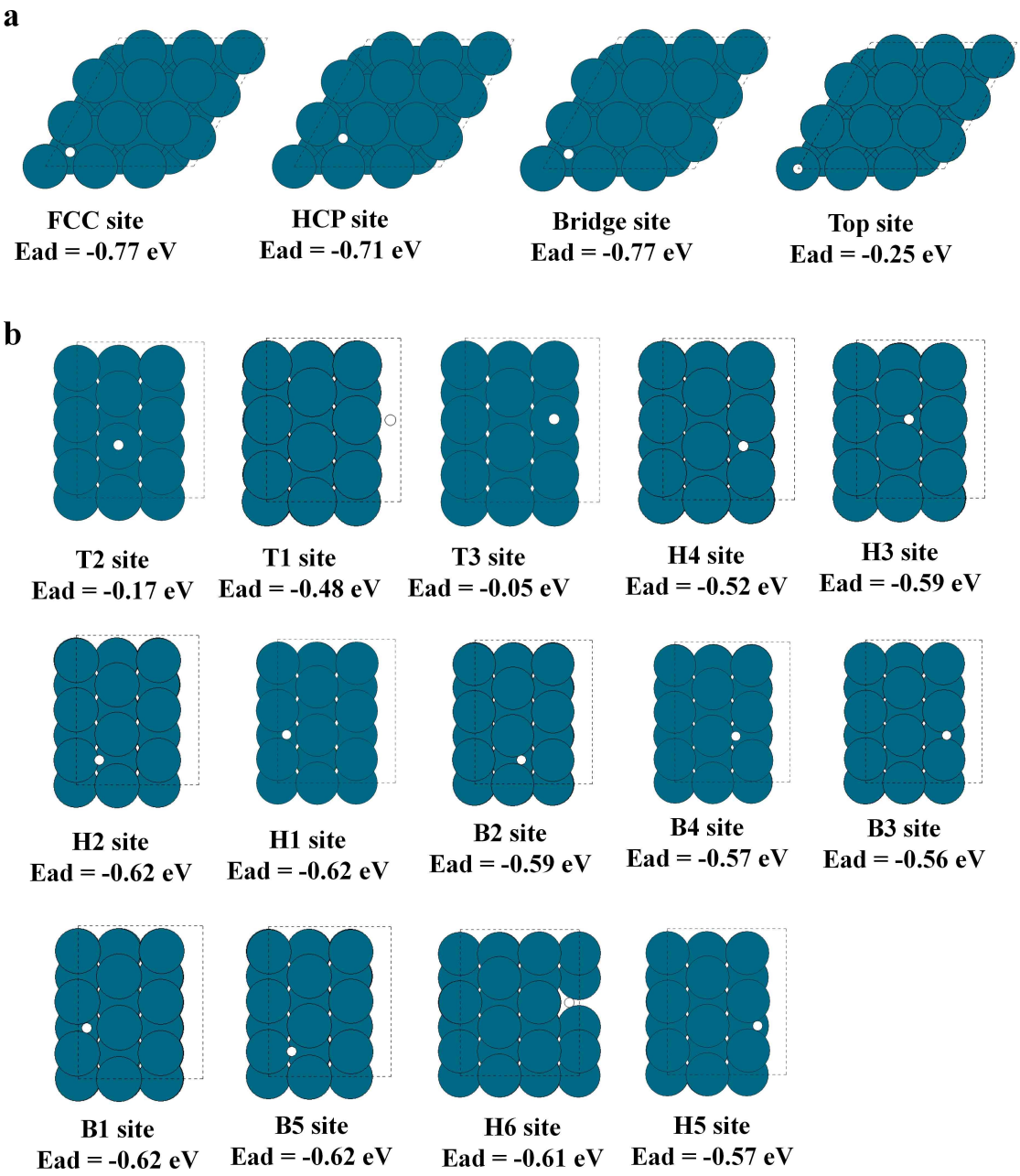

Fig. S15 | The most stable adsorption models and corresponding adsorption energy values for H adsorbed on different sites of Pd(111) (**a**) and Pd(211) (**b**).

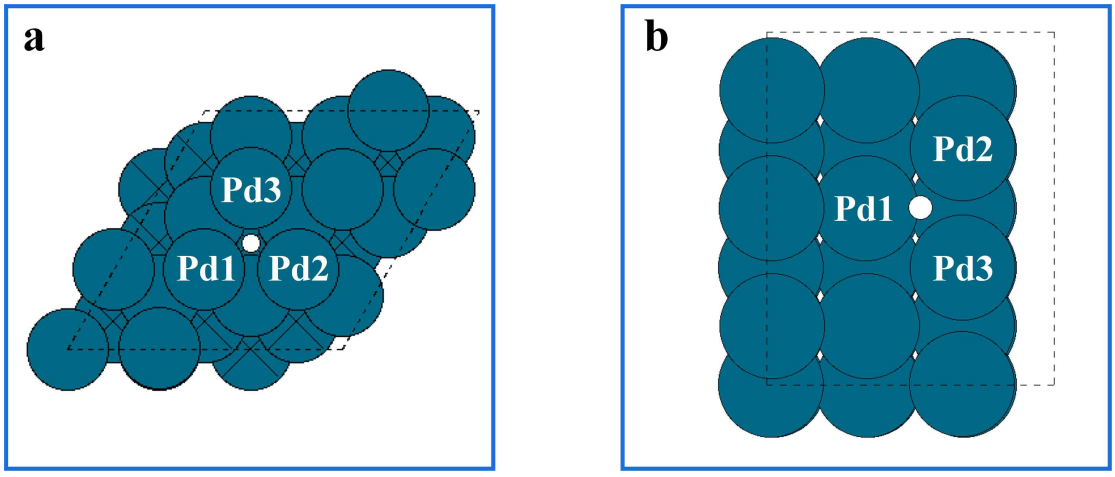

Fig. S16 | Models of 1 H* adsorbed on Pd (111) (**a**), and Pd (211) (**b**). Pd1, Pd2, and Pd3 are atoms bonded to the 1 H*.

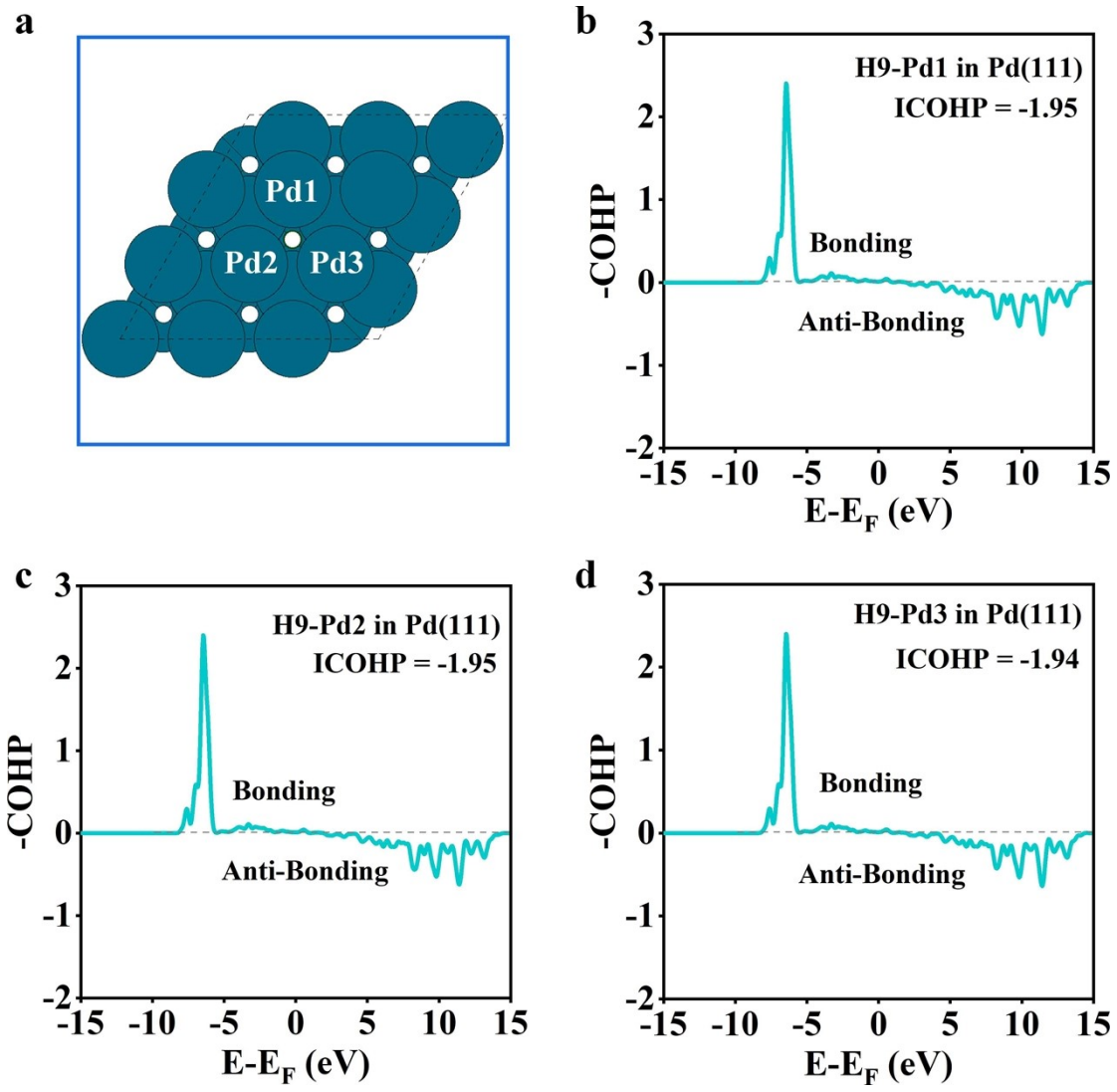

Fig. S17 | Models of high coverage H* adsorbed on Pd (111). Pd1, Pd2, and Pd3 are atoms bonded to the 9th H* (**a**), COHP for the ninth H* bonded to Pd1 (**b**), Pd2 (**c**), and Pd3 (**d**) of Pd (111).

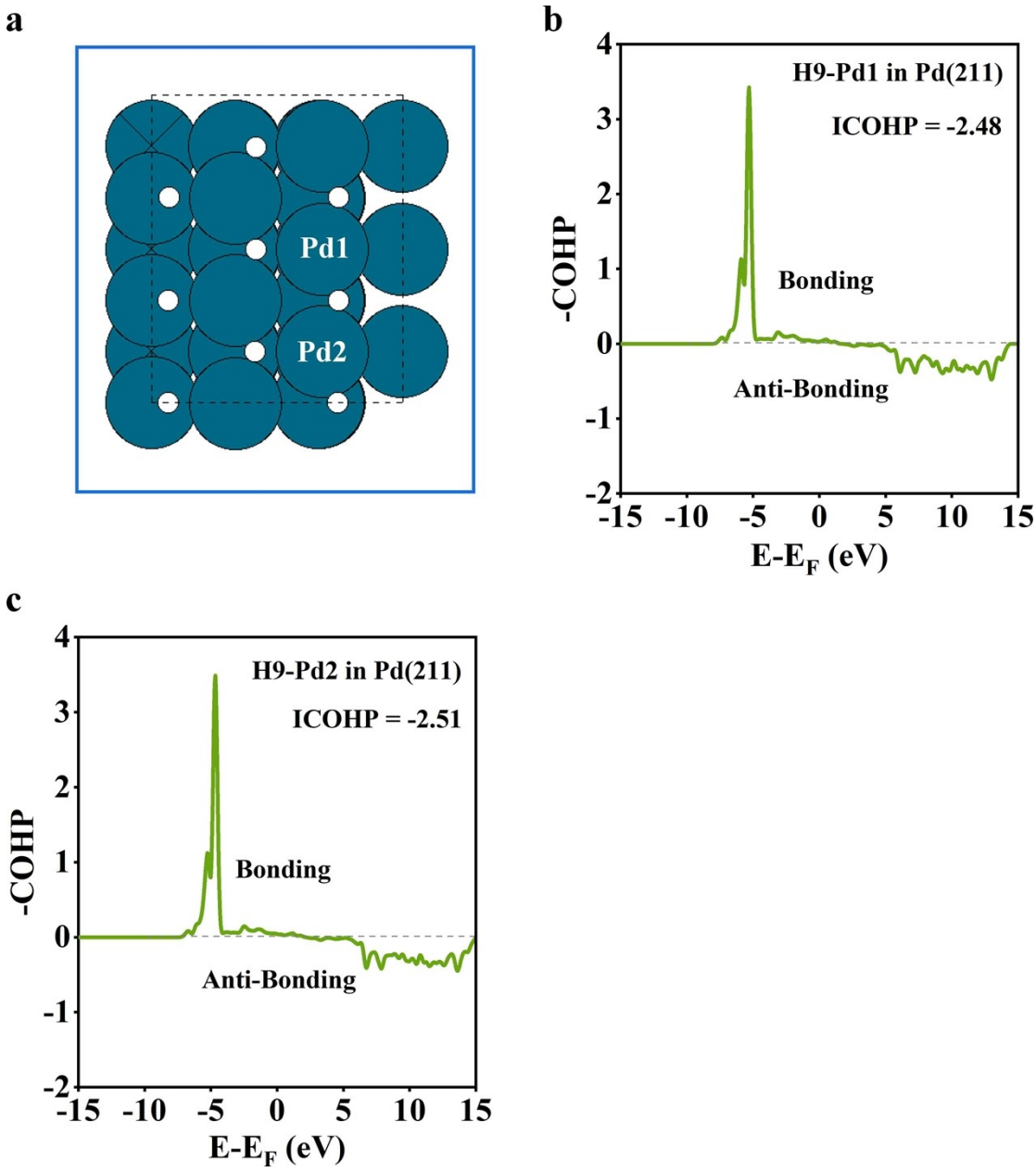

Fig. S18 | Models of high coverage H* adsorbed on Pd (211) (**a**). Pd1 and Pd2 are atoms bonded to the 9th H*. COHP for the ninth H* bonded to Pd1 (**b**), Pd2 (**c**) of Pd (211).

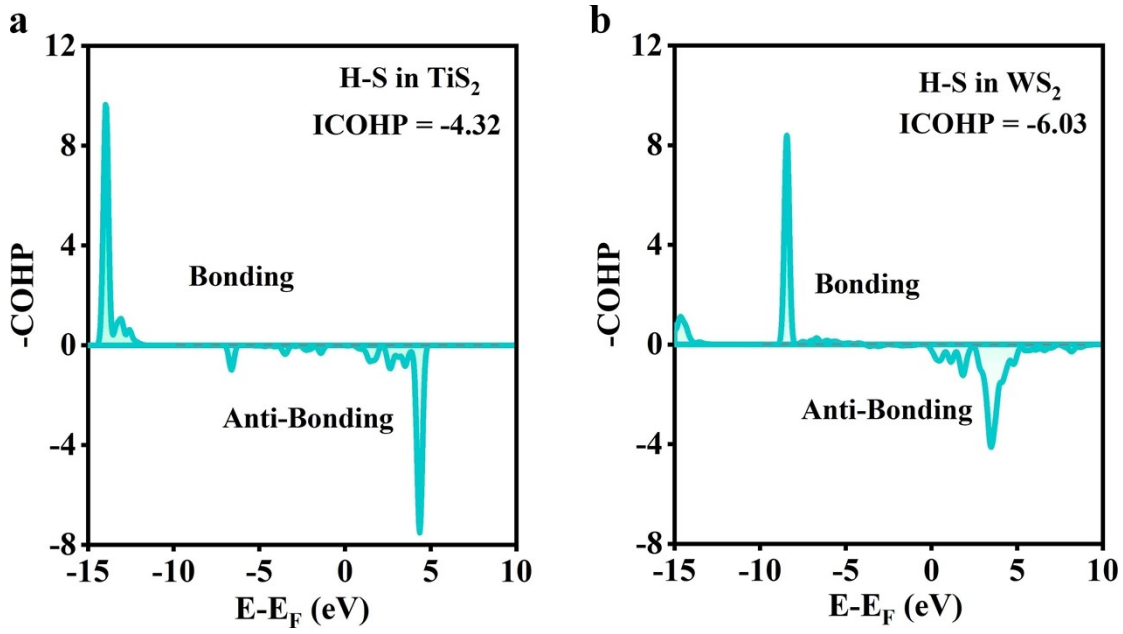

Fig. S19 | COHP for the H* and S in TiS_2 (**a**), and WS_2 (**b**).

Table S1. Comparative analysis of electrocatalytic Activity: Pd-MoS_2, Pd-WS_2, Pd-TiS_2 composites vs. previously reported Pd-decorated 2D catalysts for HER Application in 0.5M H_2SO_4.

Catalysts	η_{10} (mV)	Tafel slope (mV/dec)	Reference
Pd ND/DR-MoS_2	103	41	*J. Mater. Chem. A* 2016, **4**, 4025-4031
7.4 % Pd-MoS_2	205	91	*Appl. Surf. Sci.* 2023, **642**, 158563
Pd-MoS_2/MWCNT	120	54	*Int. J. Hydrog. Energy* 2017, **42**, 2961-2969.
1% Pd-MoS_2	89	80	*Nat. Commun.* 2018, **9**, 2120
Pd-graphene	80	46	*Int. J. Hydrog. Energy* 2015, **40**, 16184-16191
VS_2-Pd	133	75	*Inorg. Chem.* 2020, **59**, 10197-10207
Pd NWs@MoS_2	25	44	*Nano Research* 2016, **9**, 2662-2671.
VGN@$Pd_{0.2}$-MoS_2	106	60	*J. Power Sources* 2020, **456**, 227998
d-$PdTe_x$	70	116.4	*ACS Catal.* 2023,**13**, 2601−2609
Pd-MXene	149	96	*Energy Fuels* 2023, **37**, 16856–16865
$Pd_{0.1}TaS_2$	241	52.7	*J. Mater. Chem. A* 2017, **5**, 22618-22624
$Pd_{0.23}NbS_2$	157	50	*Chem. Mater.* 2019, **31**, 13, 4726–4731
Pd-MoS_2	70	43	**This work**
Pd-WS_2	113	49	**This work**
Pd-TiS_2	131	61	**This work**